

Evidence of critical dynamics in various electromagnetic precursors^{*}

S. M. Potirakis^{1,a}, Y. Contoyiannis¹, A. Schekotov²,
K. Eftaxias³, and M. Hayakawa^{4,5}

¹ Department of Electrical and Electronics Engineering, University of West Attica, Campus 2, 250 Thivon and P. Ralli, Aigaleo, Athens 12244, Greece

² Institute of Physics of the Earth, Russian Academy of Sciences, 10 Bolshaya Gruzinskaya, 123995 Moscow, Russia

³ Department of Physics, University of Athens, Panepistimiopolis, Zografos, Athens 15784, Greece

⁴ Hayakawa Institute of Seismo Electromagnetics Co. Ltd., UEC (University of Electro-Communications) Alliance Center #521, 1-1-1 Kojimacho, Chofu, Tokyo 182-0026, Japan

⁵ UEC, Advanced Wireless & Communications research Center, 1-5-1 Chofugaoka, Chofu, Tokyo 182-8585, Japan

Received 2 October 2020 / Accepted 7 October 2020

Published online 19 January 2021

Abstract. A wide variety of electromagnetic phenomena possibly related with earthquake (EQ) preparation processes have been reported in the literature during the last few decades. An interesting aspect in their study is the time series analysis of the related observables aiming at the investigation of any embedded dynamics. In this review article we focus on the study of fracto-electromagnetic emissions (fracto-EME) at the MHz band, the ultra-low frequency (ULF) magnetic field variations (<3 Hz) and the subionospheric very low frequency (VLF) propagation anomalies. We present recent analysis results for these electromagnetic signals using two independent methods which are known for their ability to uncover critical dynamics, the recently proposed method of critical fluctuations (MCF) and the natural time (NT) analysis method. Our results show that all three considered electromagnetic signals present critical characteristics from a few weeks up to a few days before the main shock occurrence. On the other hand, signatures for the departure from the critical (highly symmetrical) state towards a low symmetry state, a state during which there is high localization of the EQ preparatory process, have been identified in specific cases for the MHz fracto-EME as well as for the ULF magnetic field variations. Based on a multidisciplinary analysis, a four-stage model of EQ dynamics by means of fracto-EME in the MHz and kHz bands has recently been proposed. The hypothesis that the precursors

^{*} Supplementary material in the form of one pdf file available from the Journal web page at <https://doi.org/10.1140/epjst/e2020-000249-x>

^a e-mail: spoti@uniwa.gr

considered in this article emerge during the spatially extensive phase of EQ preparation, which corresponds to the first stage of the abovementioned four-stage model, as well as their relation with the foreshock seismic activity are discussed.

1 Introduction

The earthquakes (EQs) are shocking geophysical phenomena which refer to the release of energy when ruptures happen in the lithosphere as a result of accumulated stress sourced from plate tectonics. The intense (with magnitude ~ 6 or larger), shallow EQs which happen on land or near coastline, as well as the tsunamigenic EQs, have a very important social impact because they are often very disastrous phenomena. The main tremor requires a long preparation period before it happens suddenly, when a particular fault is not any more capable of sustaining the increasing deformation (e.g., [1]). During the last few decades, there has been published many articles reporting electromagnetic (EM) phenomena possibly related to EQs, e.g., [2–10]. Nevertheless, EM precursors are still a highly disputed topic among scientists of different disciplines. Scientific studies related to EQ precursors, and particularly in the case of short-term prediction, are often faced with intense skepticism [11]. Negative views have been extended to the extreme claim that any EM precursory activity is impossible, e.g., [12] and references therein.

It is true that the mechanisms for the generation of different EQ-related EM phenomena are not yet fully understood despite the fact that a number of suggestions have appeared in the literature, e.g., [4,5,12–20]. Beyond the statistical confirmation for the correlation of such phenomena with EQs, dealing with such a controversial subject calls for strong scientific evidence linking different facets of the EQ preparation processes with characteristics of the observed EM signals. From this point of view, the time series analysis of the possibly EQ-related EM observables aiming at the investigation of any embedded dynamics which are expected to characterize EQ-preparation processes is considered very important.

Phase transition phenomena are a very important field in statistical physics, while in the framework of modern complex systems theories they have found application to almost all sciences. A phase transition phenomenon is characterized by the transition between two phases (states) in which a system could exist. It has been proposed (e.g., [21]) that as the lithosphere system evolves towards an intense EQ can be studied from the phase transitions point of view. On the basis of the collective phenomena occurring in critical systems, it has been suggested that intense EQs result after the lithosphere has reached a kind of critical point (e.g., [22] and references therein), while critical characteristics have been identified in foreshock seismicity. Therefore, time series analysis methods capable of revealing features indicating the approach to critical point as well as the departure from it may provide evidence for the seismogenic nature of pre-EQ EM phenomena.

In this review article we present, in a unified manner, findings that have already been reported in a series of recently published papers of ours concerning the identification of critical characteristics in different EM signals prior to large EQs. We focus on two independent methods which are known for their ability to uncover critical dynamics, the recently proposed methods referred to as the method of critical fluctuations (MCF) [23–26] and the natural time (NT) analysis [27]. Their application to various EM signals is explained, while recent analysis results are presented. Specifically, we deal with three types of ground-observed EM signals: the fracto-electromagnetic emissions (fracto-EME or EME) at the MHz band, the ultra-low frequency (ULF) magnetic field variations (< 3 Hz) and the subionospheric very low frequency (VLF) propagation anomalies. We clarify that the scope of this article is to highlight the compatibility that is observed among different pre-EQ EM signals

in terms of the approach and departure from critical state. This is not an attempt to suggest that these different EM precursors are generated by the same physical mechanism or to suggest a complete EQ prediction method.

This paper is organized as follows: In Section 2, we provide information about the EM signals considered in this study. In Section 3, we briefly present the MCF and NT analysis methods, as well as the way they are applied to different EM signals. Recent analysis results concerning the examined EM signals are presented in Section 4. Finally, in Section 5, we discuss these results in the frame of the four-stage model of EQ dynamics by means of fracto-EME [12] and summarize the conclusions.

2 Electromagnetic signals under study

As already mentioned, out of the wide variety of pre-EQ EM phenomena, we focus on three specific ground-observed of them which fall within our own research experience. Namely, we are interested in the fracto-EME at the MHz band, anomalies in the ULF magnetic field variations (<3 Hz) and the subionospheric VLF propagation anomalies. In the online available supplementary material we present key information about the EM signals mentioned in this article, such as observation stations data, acquisition parameters, possible preprocessing and notations, while more detailed information can be found in the original papers the results of which we present in this review paper (see Sect. 4). In brief:

(a) In the case of MHz EME, we use custom-designed receivers and $\lambda/2$ electric dipole antennas to continuously record the electric field, in narrow bands around specific central frequencies, at multiple telemetric stations dispersed all around Greece, while the sampling frequency is $f_s = 1$ Hz (see supplementary downloadable material of [28]). Depending on the analysis method used to identify critical dynamics (see Sect. 3), the raw (unprocessed) MHz EME recordings or the so-called “energy of EM events” (each one of them corresponding to the energy of successively recorded fracto-EME values exceeding a specific threshold, cf. Sect. 3.2.2) are employed ([10,28] and its supplementary downloadable material, [29]). Note that MHz EME recordings of any time of the day (not only nighttime ones) are analyzed in search for valid MHz EME anomalies. Please refer to the online available supplementary material of this article for more information about the experimental infrastructure and the definition of the energy of EM events.

(b) In the case of the ULF magnetic field variations, we have used ground-based magnetometer data from a number of stations belonging to Japan Meteorological Agency, one station of Kyoto University and one station belonging to the Institute of Geophysics of China Earthquake Administration. In this case too, a constant sampling frequency $f_s = 1$ Hz is employed, while the data are provided in the conventional format of IAGA (International Association of Geomagnetism and Aeronomy) 2000, where the magnetic field is represented by four time series: horizontal (H) component, declination (D), vertical component (Z), and total field (F). In all cases we use local nighttime recordings during which man-made EM noise is lower (the time period is dependent on the location and the time period of the year). Depending on the employed analysis method (see Sect. 3), we use either the unprocessed magnetic field data, or five specific ULF magnetic field quantities: (i) the average power of the horizontal magnetic field component, F_h ; (ii) the average power of the vertical magnetic field component, F_z ; (iii) the ratio of the average power of the vertical over the horizontal magnetic field component, or “polarization”, $P_{z/h}$; (iv) the depression of the horizontal magnetic field component, Dep_h ; and (v) the relative daily depression of the horizontal magnetic field component δDep_h [30,31]. Please refer to the online available supplementary material for more information about the

experimental infrastructure and the definition of the abovementioned ULF magnetic field quantities.

The ULF quantities F_h , F_z , and $P_{z/h}$ have been suggested as indicators of conventional ULF radiation from the lithosphere. It should be mentioned at this point that an increase of the ULF quantities F_h , F_z , and $P_{z/h}$ cannot be simply related to lithospheric electromagnetic emissions (local phenomenon), since such an increase may be the result of a phenomenon of magnetospheric origin, such as a magnetic storm, (global phenomenon). Therefore in their use for the study of ULF variations of possible lithospheric origin, one should first try to focus on time periods when ULF variations from other sources (e.g., from magnetic storms) are not expected. For this reason, we always study geomagnetic activity (at least *Dst* index, which is a geomagnetic index which monitors the world-wide magnetic storm level, constructed by averaging the horizontal component of the geomagnetic field from mid-latitude and equatorial magnetograms from all over the world) in search for such phenomena, in parallel to the study of the abovementioned ULF parameters. Note that, even if no magnetic storm has taken place, an increase of these quantities cannot reliably be attributed to lithospheric EM radiation since it is dependent on the signal to noise ratio of the measurements and the sensitivity of sensors. Provided that a global phenomenon has been excluded, the more indicative sign for lithospheric ULF magnetic field radiation is considered the increase of $P_{z/h}$, as long as that this is not due to the local interferences or/and the horizontal field depression that has a seismo-ionospheric origin as described in the following.

The fourth ULF parameter is an indicator of another phenomenon: the non-conventional parameter Dep_h is an inverse of the average power of the horizontal magnetic field component, and is used in order to investigate the depression of ULF waves (of magnetospheric origin) observed on the ground as the ionospheric signature. Schekotov et al. [32] studied this effect based on the data during rather long periods (4 years in Russia and two years in Japan), which was proved to be an important parameter in identifying a precursor to an EQ. This phenomenon is not completely understood, but it can be interpreted in terms of enhanced absorption of downgoing Alfvén waves through the perturbed lower ionosphere [33], indicating the presence of perturbations in the lower ionosphere.

(c) In the case of subionospheric VLF propagation anomalies, we use custom-designed VLF/LF receivers (usually employing simple electrical rod –monopole– antennas) installed at stations dispersed all around Japan which monitor the signal transmitted (at discrete frequencies) from specific transmitters located both in Japan and other countries. The receiver amplitude is continuously recorded at a sampling frequency $f_s = 1$ Hz. From these recordings, we use only the (local) nighttime data, which, depending on the time periods around the year, correspond to: 10:00–20:00 UT for 22/11–21/02, 11:00–19:00 UT for 22/02–21/05, 11:30–17:30 for 22/05–21/09, and 10:30–19:00 for 22/09–21/11. Either the unprocessed receiver amplitude values, $A(t)$, or the daily values (1 value/day) of three specific quantities, characterizing the nighttime VLF propagation, namely, *TR* (“trend”), *DP* (“dispersion”), and *NF* (“night-time fluctuation”) [34,35] are used depending on the analysis method (see Sect. 3). Please refer to the online available supplementary material for more information about the experimental infrastructure and the definition of the abovementioned VLF propagation quantities.

3 Methods

In the following we briefly present the time series analysis methods employed in this article. Specifically, we present key concepts and formulae of MCF and NT analysis

methods, as well as the way they are applied to different signals. These methods have been successfully tested in many systems presenting critical dynamics, both real and numerical (including Ising models), e.g. [10,24–31,34–40]. The reader interested in an in-depth study of the theoretic background of these methods and more details on the involved concepts is referred to [23–26,36,37,41–43] for MCF and [27] for NT analysis.

3.1 Method of critical fluctuations (MCF)

As already mentioned in the introduction (Sect. 1), it has been proposed that EQ-related effects can be studied from the point of view of phase transitions. It is reminded that in a second-order phase transition the second-order derivative of the thermodynamic free energy (the energy of a system that is available to perform thermodynamic work) is discontinuous, while the first-order one is continuous, and therefore second-order phase transition is characterized by a gradual change. On the other hand, in a first-order phase transition the first order derivative of the thermodynamic free energy is discontinuous and thus it is characterized by abrupt changes. The so-called “tricritical point” is the point in the phase diagram of the system at which the two aforementioned basic kinds of phase transition meet.

It has been proposed by Contoyiannis and Diakonou [23] that a nonlinear intermittent map of the form:

$$\varphi_{n+1} = \varphi_n + u\varphi_n^z \quad (1)$$

is capable of describing the dynamics of the fluctuations of the order parameter φ at critical state. In equation (1), φ_n is the n -th sample of the scaled order parameter, $u > 0$ is a coupling parameter, and z stands for a characteristic exponent associated with the isothermal exponent δ for critical systems at thermal equilibrium ($z = \delta + 1$). Actually, in order to more realistically model a real (or numerical) dynamical system one has to add to equation (1) a non-universal uncorrelated “noise” term, ε_n , that is necessary for the establishment of ergodicity [24]. Therefore, equation (1) becomes:

$$\varphi_{n+1} = \varphi_n + u\varphi_n^z + \varepsilon_n. \quad (2)$$

Note that in the special case of tricritical dynamics, the fluctuations of the order parameter φ have been proved [26] that can be expressed by a similar nonlinear intermittent map of the following form:

$$\varphi_{n+1} = \varphi_n - u\varphi_n^{-z} + \varepsilon_n \quad (3)$$

The only difference between the maps of equations (2) and (3) is the opposite sign of both the coupling parameter and the characteristic exponent.

The key idea behind the MCF is that criticality manifest itself by a power-law distribution of properly defined laminar lengths (waiting times) l , $P(l) \sim l^{-p_l}$ [41], where the exponent p_l is $p_l = 1 + \frac{1}{\delta}$. Therefore, if one models the distribution of laminar lengths of the order parameter fluctuations by a function $f(l)$ composed by two “competing” factors, one power-law decay factor corresponding to critical dynamics, and one exponential decay factor describing memoryless, uncorrelated, noise (as will be shown by Eq. (4)), it is possible to monitor the dynamics of the order parameter fluctuations; the critical dynamics as well as the departure from the critical state, either by the emergence of tricritical dynamics or by appearance of the so-called “symmetry breaking” phenomenon (will be explained later), can be identified. Specifically, the function used in MCF to model the distribution of laminar lengths is [24]:

$$f(l) = p_1 \cdot l^{-p_2} \cdot e^{-lp_3} \quad (4)$$

Note that equation (4) can efficiently model the distribution of laminar lengths in both cases of the nonlinear intermittent maps of equations (2) and (3), which means that equation (4) can be used for the study of both kinds of dynamics. The values of the p_2 (power-law decay exponent) and p_3 (exponential decay exponent) signify the presence of critical dynamics or the departure from critical state in the following way [34,36]:

(a) $p_2 > 1$ and $p_3 \approx 0$ for a wide range of laminar regions imply predominance of critical dynamics, a second-order phase transition in equilibrium. Note that in this case the exponent p_2 is equal to the exponent, p_l so it holds that $p_2(= p_l) = 1 + \frac{1}{\delta} = \frac{z}{z-1}$. The time series excerpt satisfying these criticality conditions is usually referred to as a “critical window” (CW).

(b) $p_2 < 1$ and $p_3 \approx 0$ for a wide range of laminar regions imply departure from the critical state by means of a tricritical crossover, i.e., by passing from the second-order phase transition (high-symmetry state) to the first-order phase transition (low-symmetry state) through the vicinity of the tricritical point (an intermediate “mixing state”) [26]. Note that in this case, it has been proved [26] that $p_2(= p_l) = \frac{z}{z+1}$. The emergence of tricritical dynamics after a CW indicates departure from criticality towards a process characterized by a first-order phase transition [26].

(c) Emergence of a bimodal distribution in the fluctuations of the order parameter in parallel to (remaining) critical dynamics after a CW is the signature of the theoretically expected so-called “symmetry breaking” phenomenon, also indicating departure from criticality [36,37]. Note that in the symmetry phase there is a single fixed point (minimum of the Landau free energy $U(\varphi)$ vs. the order parameter φ) while in the broken symmetry phase there are two fixed points. Correspondingly, the distribution of the order parameter values in the first case is of unimodal form (one lobe), while in the second case is of bimodal form (two lobes). This happens because a fixed point attracts a high number of values of the order parameter close to it determining the form of the distribution. If such a situation is observed after a CW, the MCF analysis should still detect indications of critical dynamics until the complete departure from critical state (as soon as the two lobes of the bimodal distribution become completely separated). Therefore, the corresponding laminar lengths distribution should be fitted by equation (4) with $p_2 > 1$ and $p_3 \approx 0$ (critical dynamics signature) at least for a very narrow range of laminar regions (or even for just one laminar region). This phenomenon signifies the transition from a highly symmetrical state (critical state), to a low symmetry state, during which the process is focused around “preferred” directions. The marginal presence of power-law distribution indicates that the system’s state is still close to the critical point.

It is highlighted that the detection of critical state followed by the detection of the departure from the critical state, is a very important combination of phenomena which may serve as short-term prediction of the time of occurrence of a future major EQ, as well as for the discrimination of the main (strongest) event from its strong foreshocks [36] (see also Sect. 4).

The application of MCF comprises six simple steps [34]:

(1) Find a part of the time series with adequate length ($> \sim 5000$ values) presenting, at least, local stationarity, by checking the cumulative mean value of the time series using nested time series excerpts of progressively wider length.

(2) Calculate the histogram of the order parameter φ (which is usually the original time series values).

(3) Determine a value from the histogram as the fixed-point φ_o , which will serve as the “start of laminar regions”. The fixed point in one-dimensional iterative maps like the map described by equation (2) is determined according to the turning point method [42,43]. According to the specific method, the fixed point lies in the side of

the probability distribution where the higher probability of occurrence appears. In fact, this is the edge of the most “abrupt” side.

(4) For a number of different values within the φ amplitude range, which are called “ends of laminar regions” and denoted as φ_l , calculate the distribution $P(l)$ of the “laminar lengths” of each corresponding laminar region (φ_o, φ_l); one distribution per φ_l value. Laminar lengths are the waiting times within each laminar region (φ_o, φ_l), in other words the number of successive φ -values obeying the condition $\varphi_o < \varphi < \varphi_l$. Note that all values within the φ amplitude range are examined as possible end points, while the examination is performed exhaustively by progressively increasing the number of equally spaced values covering the whole amplitude range. An empirical rule is checked before proceeding to the next step: the calculated distributions $P(l)$ should take non-zero values at least up to $l = 20 - 30$. If this rule is not satisfied, this means that it is necessary to add uniform noise as described in the next step (5) and then repeat steps (2)–(4), otherwise proceed to step (6).

(5) If necessary (according to the criterion of step 4) add uniform noise in the range $[-\varepsilon_0, \varepsilon_0]$, with ε_0 of the order of 10^{-2} and repeat steps (2)–(4). The uniform noise is added after normalizing the original time series values of the time window under analysis in the range $[0, 1]$, to numerically fit the problem to the nonlinear map of either equation (2) or equation (3). Consequently, the normalized time series values plus the uniform noise becomes the order parameter φ for the execution of steps (2)–(4). Note that for the non-linear map of equation (2) with $z = 4$ within the range $[0, 1]$ it has been found that the appropriate value was $\varepsilon_0 = 0.0175$ [24]. However, for the case of real time series MCF steps (2)–(4) are initially applied directly to the original time series values with no addition of any noise ($\varepsilon_0 = 0$). But if the rule mentioned in step (4) is not satisfied, then an appropriate value of $\varepsilon_0 > 0$, of the order of 10^{-2} , is determined by fine tuning and added to the normalized time series values before re-executing steps (2)–(4).

(6) Plot each one of the obtained distributions $P(l)$ on a log-log plot and by fitting it using the function $f(l)$ of equation (4), determine a set of exponents p_2, p_3 for each laminar region. The dynamics are identified by the consistent behavior of the exponent values according to the cases (a)–(c) described above. In particular, as regards the range of end points for which the exponent values’ conditions of cases (a) or (b) are satisfied, the wider the range is, the clearest the signature of criticality (case (a)) or tricriticality (case (b)) is.

3.1.1 MCF application to fracto-electromagnetic emissions

The MCF is directly applied to the MHz EME recordings without any pre-processing (e.g., [10,26,38–40]). This means that the order parameter φ corresponds to the original time series values of the recorded electric field (cf. Sect. 2). The six step MCF application procedure is step by step applied as described in Section 3.1 (e.g., Fig. 1). If necessary, according to the criterion of step (4) (cf. Sect. 3.1), uniform noise might be added to the original time series values. However, in most cases there is no need for uniform noise addition to reveal the embedded dynamics (e.g., [10,26,38–40]).

3.1.2 MCF application to ultra-low frequency magnetic field variations

In the case of ULF magnetic field recordings, MCF is also directly applied to the recordings without any pre-processing [30,36]. This means that the order parameter φ each time corresponds to the original recorded values of one of the magnetic field time series: horizontal (H) component, declination (D), vertical component (Z), or total

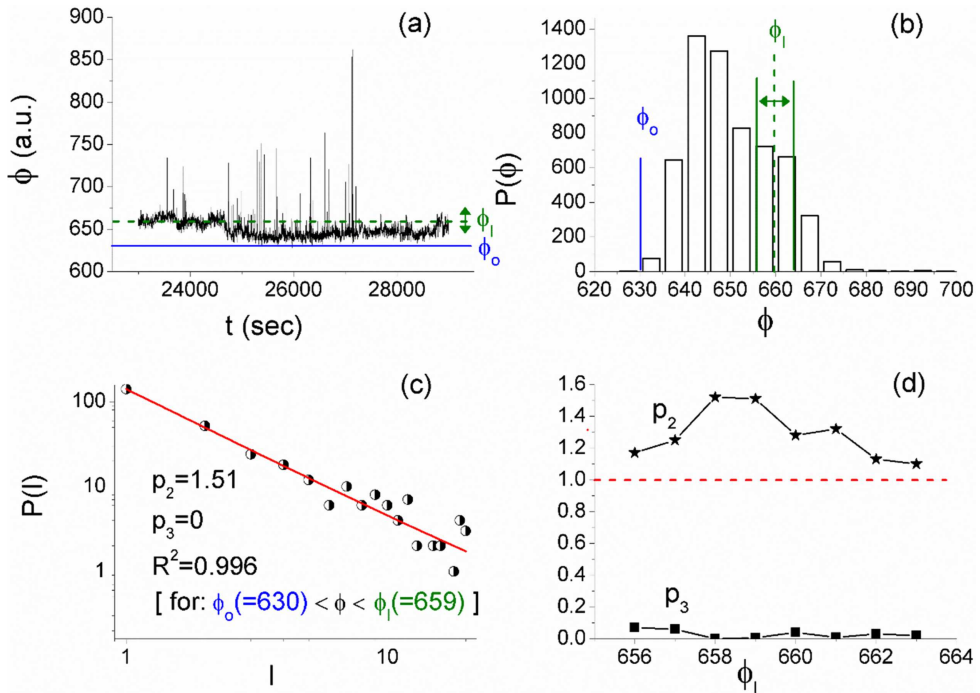


Fig. 1. A typical example of the results obtained after the application of MCF to MHz EME [40]. (a) A 1.7 h-long (6000 samples) excerpt of the MHz EME time series recorded on 1 June 2017 (06:23:20–08:03:20 UT) at the Lesvos island station before the Lesvos 12 June EQ (of the 2017 eastern Aegean Sea EQs) (cf. Sect. 4.1). The horizontal solid and dashed lines indicate the φ_o and φ_l values, respectively, that have been used to calculate the laminar lengths, the distribution of which is presented as an example in (c). (b) Amplitude distribution of the signal of (a). The fixed φ_o value and the range of φ_l values used in the MCF analysis of (a) are shown by vertical lines. (c) A representative example of laminar distribution and the involved fitting for the laminar region $\varphi_o (=630) < \varphi < \varphi_l (=659)$. The solid line corresponds to the fitted function (cf. Sect. 3.1). (d) The obtained exponents p_2 , p_3 vs. different values of the end of laminar region φ_l . The horizontal dashed line indicates the critical limit ($p_2 = 1$). Critical behavior is obvious (cf. Sect. 3.1).

field (F) (cf. Sect. 2). In contrast to the case of MHz EME, in most applications of MCF to ULF magnetic field data it proved to be necessary, according to the criterion of step (4) (cf. Sect. 3.1), to add uniform noise to the original time series values in order to reveal the embedded dynamics [30,36].

Note that the ULF magnetic field quantities F_h , F_z , P_z/h , Dep_h and δDep_h employed by conventional statistical analysis (e.g., [44–46]) (cf. Sect. 2 and the online available supplementary material) cannot be used with MCF. The reason is that, as already mentioned in Section 3.1, a time series of at least ~ 5000 values are necessary for MCF to produce reliable results while these quantities are only available in daily values.

3.1.3 MCF application to subionospheric very low frequency propagation anomalies

The use of the daily subionospheric parameters TR , DP , and NF employed by the conventional nighttime fluctuation method [47] (cf. Sect. 2 and the online available supplementary material) is not possible with MCF for the reason that, as already mentioned

in Section 3.1, a time series of at least ~ 5000 values are necessary for MCF to produce reliable results. Therefore, the analysis has to be performed on the nighttime unprocessed (raw) amplitude, $A(t)$, on reception. In most cases, the VLF subionospheric path data present a “normal” variation comprising a slower component over which a higher frequency, low amplitude, fluctuation exists [34]. For these cases, the MCF is applicable as usual to the raw amplitude data, as in the case of MHz EME, i.e., directly to stationary parts of the original time series (cf. Sect. 3.1.1) [34].

However, for some VLF subionospheric path data the usual way of application of MCF is not always possible. The reason is that in some cases the signal is dominated by artificial, transmitter-induced, variations. Specifically, sudden bi-level changes “modulated” by a slower component, as well as higher frequency, low amplitude, fluctuations, were identified in the signal of stations using simple electrical rod (monopole) antennas during specific time periods [34]. Note that these sudden bi-level changes separate the receiver amplitude data into two sets of fluctuations the “upper” and the “lower” fluctuations [34]. The described “abnormal” variation was observed only in the signal received from a specific transmitter (the JJI transmitter cf. Section 2 and the online available supplementary material), while it was verified that they were artificially produced by an intermittent operation of the transmitter and were irrelevant to any EQ-preparation-induced lower ionosphere anomalies [34].

In the case of the abovementioned VLF subionospheric path data, the MCF was applied to pre-processed (not raw) nighttime reception amplitude data. After investigating different ways of filtering out the artificial sudden bi-level changes, we concluded that the most efficient, in terms of reliability of MCF results, was to search for time series excerpts stationary enough to clearly reveal the existence of the lower and higher fluctuations in terms of a bimodal distribution in the fluctuations of raw receiver amplitude. Then, the upper or the lower fluctuations can easily be separated by appropriate thresholding and MCF can be applied in the usual way (cf. Sect. 3.1.1) to any of them.

3.2 Natural time (NT) analysis

The natural time (NT) analysis method was originally proposed for the analysis of ULF (≤ 1 Hz) SES (Seismic Electric Signals) [48–50], and has been shown to be optimal for enhancing the signals in the time-frequency space [51]. The transformation of a time-series of “events” from the conventional time domain to NT domain is performed by ignoring the timestamp of each event and retaining only their normalized order (index) of occurrence. Explicitly, in a time series of N successive events, the natural time, χ_k , of the k event is the index of occurrence of this event normalized by dividing by the total number of the considered events, $\chi_k = k/N$. On the other hand, the “energy”, Q_k of each k event is preserved. We note that the quantity Q_k represents different physical quantities for various time series [27], e.g., for EQ time series it has been assigned to a seismic energy released (e.g., seismic moment) [50], and for SES signals that are of dichotomous nature [4] it corresponds to SES pulse duration [49], while for geophysical scale MHz EME signals that are of non-dichotomous nature, it has been attributed to the energy of fracto-electromagnetic emission events as defined in Potirakis et al. [29] (see also the online available supplementary material). The transformed time series (χ_k, Q_k) is then studied through the normalized power spectrum $\Pi(\varpi) = \left| \sum_{k=1}^N p_k \exp(j\varpi\chi_k) \right|^2$ where ϖ is the natural angular frequency $\varpi = 2\pi\phi$ with ϕ standing for the frequency in NT termed “natural frequency”, and $p_k = Q_k / \sum_{n=1}^N Q_n$ corresponds to the k event’s normalized energy. Note that the term “natural frequency” should not be confused with the rate at which

a system oscillates when it is not driven by an external force; it defines an analysis domain dual to the NT domain in the framework of Fourier-Stieltjes transform [27].

The study of $\Pi(\varpi)$ at ϖ close to zero reveals the dynamic evolution of the time series under analysis. This is because all the moments of the distribution of p_k can be estimated from $\Pi(\varpi)$ at $\varpi \rightarrow 0$ [52]. Aiming to that by the Taylor expansion $\Pi(\varpi) = 1 - \kappa_1 \varpi^2 + \kappa_2 \varpi^4 + \dots$ the quantity κ_1 is defined where $\kappa_1 = \sum_{k=1}^N p_k \chi_k^2 - \left(\sum_{k=1}^N p_k \chi_k\right)^2$ i.e., the variance of χ_k weighted for p_k characterizing the dispersion of the most significant events within the “rescaled” interval $(0, 1]$ Moreover the entropy in NT S_{nt} is defined [53] as $S_{nt} = \sum_{k=1}^N p_k \chi_k \ln \chi_k - \left(\sum_{k=1}^N p_k \chi_k\right) \ln \left(\sum_{k=1}^N p_k \chi_k\right)$ and corresponds [27,53] to the value at $q = 1$ of the derivative of the fluctuation function $fl(q) = \langle \chi^q \rangle - \langle \chi \rangle^q$ with respect to q (while κ_1 corresponds to $fl(q)$ for $q = 2$) It is a dynamic entropy depending on the sequential order of events [53] The entropy S_{nt-} obtained upon considering [53] the time reversal T , i.e., $T p_m = p_{N-m+1}$, is also considered

A system is considered to approach criticality when the parameter κ_1 converges to the value

$$\kappa_1 = 0.070 \quad (5)$$

and at the same time both the entropy in NT and the entropy under time reversal satisfy the condition [54]:

$$S_{nt}, S_{nt-} < S_u = (\ln 2/2) - 1/4 \quad (6)$$

where S_u stands for the entropy of a “uniform” distribution in NT [53]. It has to be mentioned that the criterion of the $\kappa_1 = 0.070$ value has originally been derived for SES activity and later on the basis of the Ising model [27,52]. Its validity has been confirmed on real SES time series while it has also been verified to be valid for several self-organized criticality (SOC) models and real time series of a variety of applications [27,52]. In all these dynamical systems it has been found that the value $\kappa_1 = 0.070$ can be considered as quantifying the extent of the organization of the system at the onset of the critical stage [27].

Beyond the seismic electric signals (SES) of Varotsos’ group, the NT method has already been successfully applied on other EM variations possibly related to EQs, such as MHz–kHz EME [10,28,29], ground-observed ULF magnetic fields (e.g., [31,46,55,56]) and VLF subionospheric propagation data [35].

3.2.1 NT application to seismicity

In the special case of NT analysis of foreshock seismicity [48,50,53,57] the temporal evolution of the parameters κ_1 , S_{nt} , S_{nt-} , and one more quantity defined in the following ($\langle D \rangle$), is studied as new events that exceed a magnitude threshold M_{thres} are progressively included in the analysis. Specifically, as soon as one more event is included, first the time series (χ_k, Q_k) is rescaled in the NT domain, since each time the k event corresponds to a NT $\chi_k = k/N$, where N is the progressively increasing (by each new event inclusion) total number of the considered successive events; then all the parameters involved in the NT analysis are calculated for this new time series; this process continues until the time of occurrence of the main event [48,50,53,57].

The seismicity is considered to be in a true critical state, a “true coincidence” is achieved, when three additional conditions, further to the criticality conditions of equations (5) and (6), are satisfied: (i) The “average” distance $\langle D \rangle$ between the curves of normalized power spectra $\Pi(\varpi)$ of the evolving seismicity and the theoretical estimation of $\Pi(\varpi)$, $\Pi_{\text{critical}}(\varpi) = \left(\frac{18}{5\varpi^2}\right) - \left(\frac{6\cos\varpi}{5\varpi^2}\right) - \left(\frac{12\sin\varpi}{5\varpi^3}\right)$, $\Pi_{\text{critical}}(\varpi) \approx 1 - \kappa_1 \varpi^2$,

for $\kappa_1 = 0.070$ should be smaller than 10^{-2} , i.e., $\langle D \rangle = \langle |\Pi(\varpi) - \Pi_{critical}(\varpi)| \rangle < 10^{-2}$ (this is a practical criterion for signaling the achievement of spectral coincidence) [27]; (ii) the parameter κ_1 should approach the value $\kappa_1 = 0.070$ “by descending from above”, i.e., before the main event the parameter κ_1 should gradually decrease until it reaches the critical value 0.070 (this rule was found empirically) [27,48]; (iii) Since the underlying process is expected to be self-similar the time of the true coincidence should not vary upon changing (within reasonable limits) either the magnitude threshold M_{thres} or the area used in the calculation.

It should be clarified that in the case of NT analysis of foreshock seismicity, the introduction of magnitude threshold M_{thres} excludes some of the weaker EQ events (the ones with magnitude below this threshold) from the NT analysis. On one hand, this is necessary: depending on the installed seismographic network characteristics, a specific magnitude threshold, M_C , is usually defined to assure data completeness, so M_{thres} should be higher than M_C . On the other hand, the use of various magnitude thresholds $M_{thres} (>M_C)$ offers a means of more accurate determination of the time when criticality is reached. In some cases, it happens that more than one time-points may satisfy the rest of NT critical state conditions, however the time of the true coincidence is finally selected by the last condition that “true coincidence should not vary upon changing (within reasonable limits) either the magnitude threshold M_{thres} or the area used in the calculation”.

3.2.2 NT application to fracto-electromagnetic emissions

The application of NT analysis to MHz EME has been addressed for the first time in [29] and since then has been applied to more cases of MHz EME recorded prior to recent significant EQs [10,28]. One of the most important issues in applying NT analysis is the definition of the quantity Q_k . In the case of MHz EME this has been attributed to the energy of fracto-electromagnetic emission events or “energy of EM events”. The main idea is that clipping out the background noise level, the resulting amplitude difference is considered to correspond to fracture-related emissions and consequently it is referred to as the amplitude of “fracto-electromagnetic emission”. In this respect, the amplitude of “fracto-electromagnetic emission” can be used to obtain EM energy release related to fracture process. Specifically, each group of successively recorded values of the MHz EME exceeding a specific threshold value are considered to correspond to one EM event. The energy corresponding to each EM event, which is considered to be the quantity Q_k of the NT analysis, is calculated as the summation of the consecutive squared amplitudes of the corresponding “fracto-electromagnetic emissions”. A more detailed description of the abovementioned notions and quantities can be found in [29] and in the online available supplementary material of this article.

After the basic quantities of the NT analysis have been determined the NT analysis is applied to the revealed EM events as described in Section 3.2. The analyzed time series excerpt is considered to approach criticality when the criticality conditions of equations (5) and (6) are satisfied.

It should be noted that the MHz EME time series in most cases are not in the form of clearly distinguishable bursts, therefore there is not an easy way to define a background noise level which could be used as the abovementioned threshold. In this case, it has been proposed [29] that an exhaustive search should be performed for the determination of the threshold value. This way one can exclude thresholds that may not lead to reliable κ_1 values because of possible contamination by uneliminated noise [29]. The key idea behind this approach is that if the time series excerpt under analysis presents criticality characteristics, then there should be at least one threshold value for which the natural time criticality conditions (Eqs. (5) and (6)) are satisfied

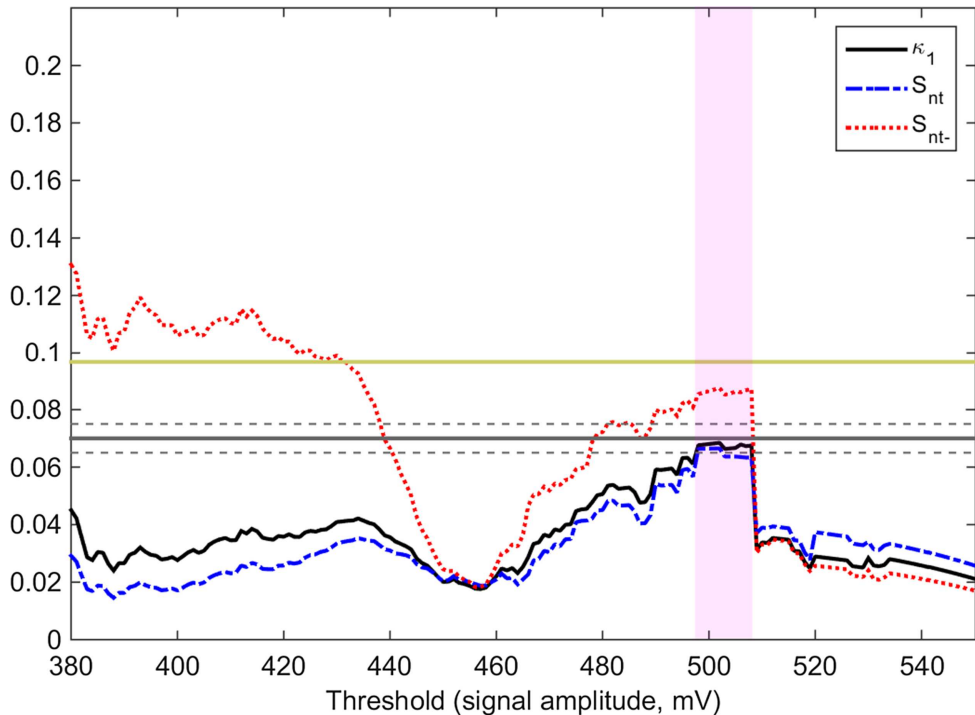


Fig. 2. A typical example of NT analysis results obtained for the Mhz EME [10]. Specifically, these correspond to the signal recorded at Zante station prior to 2014 Cephalonia EQ2 on 28 January 2014 (03:53:20–08:53:20 UT) (cf. Sect. 4.1). The quantities κ_1 (solid curve), S_{nt} (dash-dot curve), and S_{nt-} (dot curve) vs. amplitude threshold for the Mhz signal are shown. The entropy limit of S_u (≈ 0.0966), the value 0.070 and a region of ± 0.005 around it is denoted by the horizontal solid light green, solid grey and the grey dashed lines, respectively. The shaded area indicates the thresholds range for which criticality conditions according to the NT analysis method are satisfied (cf. Sect. 3.2). (For interpretation of the references to colors, the reader is referred to the online version of this paper).

(e.g., Fig. 2). If there is no such threshold, then the specific excerpt does not present criticality [29].

3.2.3 NT application to ultra-low frequency magnetic field variations

In the case of NT analysis we are not using the raw ULF data, as in the MCF case, but we use specific ULF magnetic field quantities which are usually employed in conventional statistical analysis (e.g., [44–46]) (cf. Sect. 2). Specifically, by applying a particular pre-processing procedure (described in detail in the online available supplementary material) on the raw (IAGA 2000 format) ULF data [31,44], we obtain daily values for the following ULF magnetic field quantities starting from the raw H and Z time series: (i) average power of the horizontal magnetic field component, F_h , (ii) average power of the vertical magnetic field component, F_z , (iii) ratio of the average power of the vertical over the horizontal magnetic field component, or “polarization”, $P_{z/h}$, (iv) depression of the horizontal magnetic field component, Dep_h , and (v) relative daily depression of the horizontal magnetic field component, δDep_h (see also Sect. 2).

Then, NT analysis is applied to the abovementioned ULF quantities as for the case of seismicity (cf. Sect. 3.2.1). Specifically, each daily value which is above a certain threshold is considered an event. In all ULF quantities cases (F_h , F_z , $P_{z/h}$, Dep_h , δDep_h), the “energy” of the event that is the value of the quantity Q_k , is considered to be equal to the corresponding value of each one of above quantities, provided that this is higher than a certain threshold such as $F_{h,\text{thres}}$, $F_{z,\text{thres}}$, $P_{z/h,\text{thres}}$, $\text{Dep}_{h,\text{thres}}$, and $\delta\text{Dep}_{h,\text{thres}}$, respectively. The analysis starts from a specific date and all natural time analysis parameters (κ_1 , S_{nt} , S_{nt-} , $\langle D \rangle$), cf. Sects. 3.2 and 3.2.1) are calculated from the time series rescaled in the natural time domain each time a new event is added. The analysis stops at the day of main shock. This way, calculation of the involved NT analysis parameters is repeated as many times as the total number of the events revealed through the thresholding phase, while finally an equal number of sets of these parameters are obtained and their evolution in natural time is plotted and assessed. The analyzed ULF quantity is considered to reach criticality, a “true coincidence” is achieved, if all five criticality conditions considered in the case of NT analysis of foreshock seismicity (cf. Sect. 3.2.1) are satisfied (e.g., Fig. 3).

It should be noted that although the selection of thresholds involved is arbitrary (usually more than 20 threshold values equispaced between zero and a maximum threshold value, larger than the 50% of the maximum value of the examined ULF quantity, are considered), if criticality conditions are met in close dates for more than one of the considered threshold values, then this is considered to be an indication of the validity of the performed analysis. This is because the underlying process is expected to be self-similar.

3.2.4 NT application to subionospheric very low frequency propagation anomalies

In the case of NT analysis of the VLF subionospheric propagation data, similarly to the ULF magnetic field data case (cf. Sect. 3.2.3), we are not using the unprocessed (raw) amplitude on reception, as happens with MCF analysis. In contrast, we use three specific VLF propagation quantities, characterizing the nighttime VLF propagation, which are employed in the conventional nighttime fluctuation method [47]. Specifically, we apply a particular pre-processing procedure (described in detail in the online available supplementary material) to the raw amplitude on reception to obtain daily values for the following VLF propagation quantities: namely, TR (“trend”), DP (“dispersion”), and NF (“nighttime fluctuation”) [35].

Since the ionosphere is known of being sensitive not only to pre-EQ processes, but also to a variety of different kinds of phenomena such as solar flares, magnetic storms, typhoons, tsunamis, and volcano eruptions, e.g., [16,58,59], the starting time of the analysis has to be determined after the occurrence of such kind of phenomena. This is because, if the NT analysis intended to examine the possibly EQ-related behavior of the ionosphere starts before a non-EQ-preparation-related phenomenon which undergoes a critical state, this might cause “masking” of the possible critical behavior of the ionosphere due to any EQ preparation processes. Therefore, we first apply the conventional nighttime fluctuation method [47] which can easily detect the disturbance in nighttime VLF propagation characteristics due to any phenomenon and use its results to set the initial time point for NT analysis at least a few (e.g., ~ 5) days after the day for which any normalized nighttime VLF propagation characteristic has exceeded the limit of $\pm 2\sigma$.

Then, we apply the NT method to the nighttime VLF propagation characteristic quantities TR , DP , and NF , as described in [35], in a similar way to that for the ULF magnetic field quantities presented in Section 3.2.3. Specifically: (i) We consider each daily value which is above a certain threshold as an event. In our nighttime

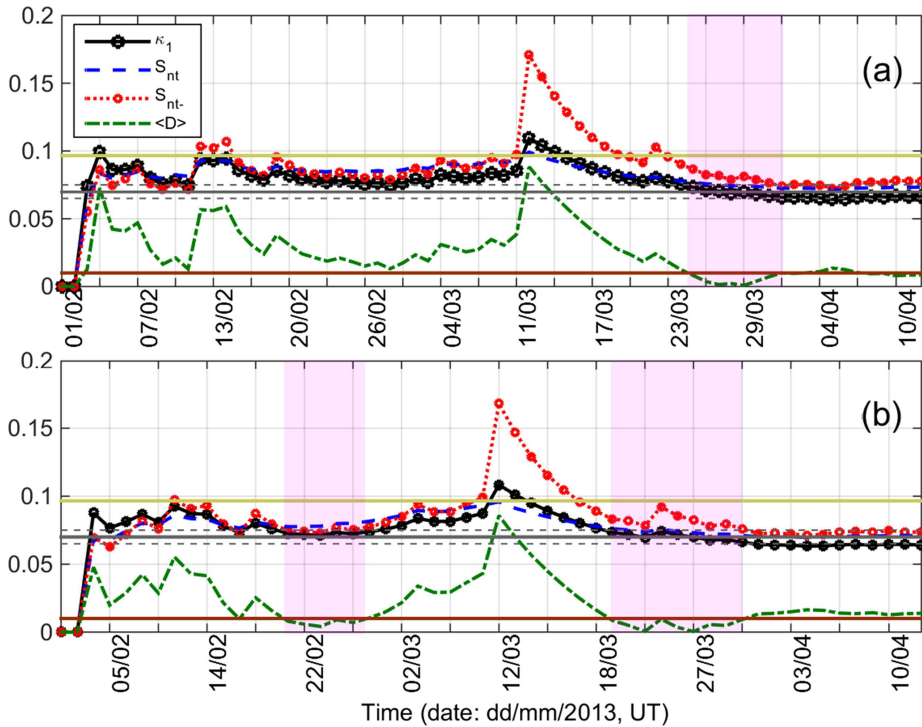


Fig. 3. A typical example of NT analysis results obtained for daily valued ULF magnetic field quantities [56]. The results correspond to the analysis of the ULF quantity F_z as based on the magnetic field recordings prior to the 2013 Kobe EQ (cf. Sect. 4.2) at SGA station for the time period from 1 February to 12 April 2013: Variations of the natural time analysis parameters for the different thresholds $F_{z,\text{thres}}$ 0.00250 (a) and 0.00375 (b), respectively. The shaded areas indicate the time range for which criticality conditions according to the NT analysis method are satisfied (cf. Sect. 3.2.1). Note that the events employed depend on the considered threshold. Moreover, the time (x -) axis is not linear in terms of the conventional date of occurrence of the events, since the employed events appear equally spaced relative to x -axis as the natural time representation demands, although they are not equally spaced in conventional time. (For interpretation of the references to colors, the reader is referred to the online version of this paper.)

VLF propagation characteristic quantities cases (TR , DP , and NF), the “energy” of k event that is the value of the quantity Q_k of NT analysis (see Sect. 3.2) is considered to be equal to the corresponding non-normalized value of each one of above quantities, provided that this is above a certain threshold such as TR_{thres} , DP_{thres} , and NF_{thres} , respectively. (ii) Then, the NT analysis is performed as in the case of pre-EQ seismic activity (cf. Sect. 3.2.1) on the revealed “events”. Starting from a specific day, all the parameters (κ_1 , S_{nt} , S_{nt-} , $\langle D \rangle$), defined in Sects. 3.2 and 3.2.1) are calculated for the time series of events rescaled in the NT domain each time a new event is added, checking for the corresponding criticality criteria as presented in Section 3.2.1 for the case of seismicity.

4 Recent results

In the following we review some recently published results [10,28,30,31,34–36,40,46,55,56] concerning evidence of critical dynamics which have been revealed by the

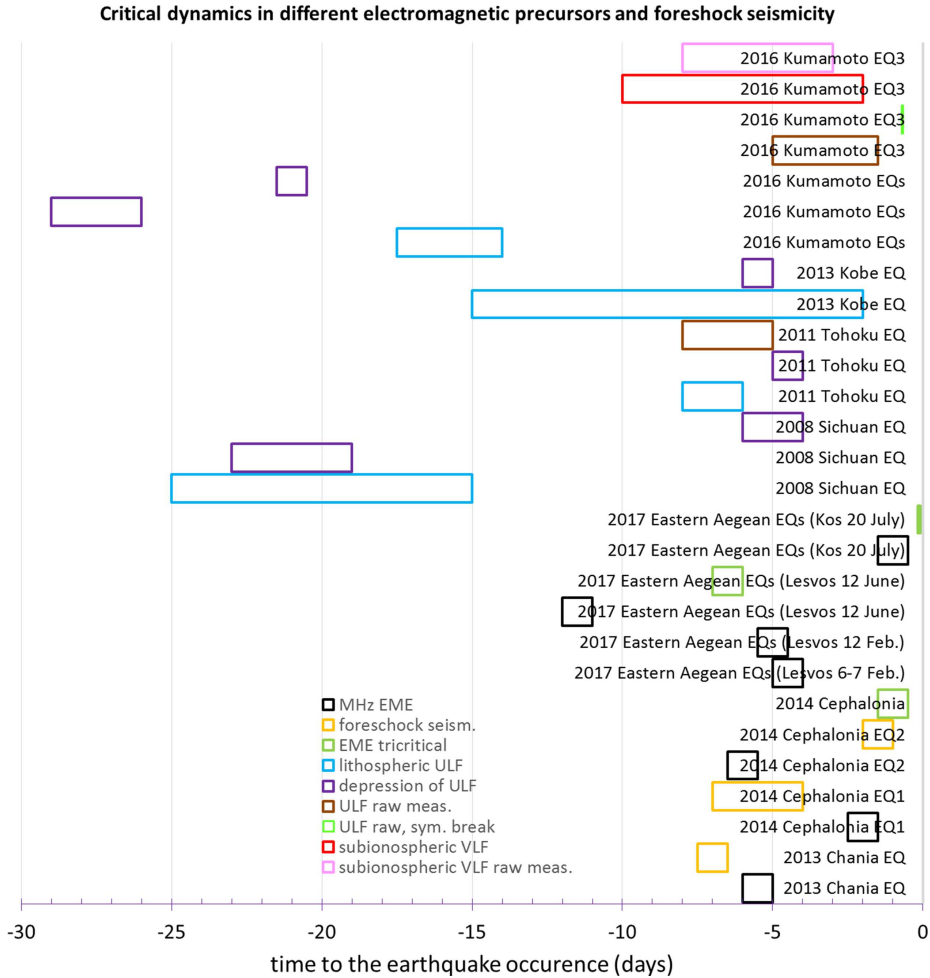


Fig. 4. Critical dynamics features revealed by MCF and NT analysis methods embedded in the time series of different EM signals as well as foreshock seismicity for a number of recent EQs which took place in Greece, China and Japan (see also text of Sects. 4.1–4.3). (For interpretation of the references to colors, the reader is referred to the online version of this paper).

MCF and NT analysis methods in the EM signals studied in this article. In all cases criticality appears a few days up to \sim one month before the occurrence of the main seismic event, while in some cases evidence for the departure from critical state have also been found as approaching to the main event. The results which are presented in the following subsections are summarized in Figure 4. For details on the EM signals studied in this article, as well as on how are the MCF and NT analysis methods applied to these different signals see Sections 2 and 3, respectively.

4.1 Results for MHz fracto-electromagnetic emissions

Evidence of criticality in MHz EME, as well as departure from critical state, have recently been reported [10,28,40] for a number of recent EQs which took place in Greece. It is also interesting to mention that foreshock seismicity was also found to

Table 1. The 2017 eastern Aegean Sea EQs.

Date –Time	Long.	Lat.	Depth	M_L
Lesvos 6–7 Feb. EQs				
6 February 2017 (03:51:41.6 UT)	39.51° N	26.10° E	14 km	5.0
6 February 2017 (10:58:02.5 UT)	39.51° N	26.12° E	15 km	5.1
7 February 2017 (02 24 04.6 UT)	39.49° N	26.11° E	16 km	5.2
Lesvos 12 Feb. EQ				
12 February 2017 (13:48:16.5 UT)	39.51° N	26.14° E	12 km	4.9
Lesvos 12 June EQ				
12 June 2017 (12:28:38.2 UT)	38.84° N	26.36° E	12 km	6.1
Kos 20 July EQ				
20 July 2017 (22:31:11.7 UT)	36.96° N	27.43° E	10 km	6.2

reach criticality at about the same period for which critical dynamics were identified in the MHz EME. Specifically, we refer to the following significant EQs:

(1) An EQ which occurred on 2013 in south-west Greece, near the west coast of Chania prefecture of the Island of Crete [(35.5° N, 23.28° E), 12 October 2013 (13:11:53 UT), $M_w = 6.4$, depth = 65 km] [28]. We shall refer to the specific EQ as “the 2013 Chania EQ”.

(2) Two EQs which occurred on 2014 in mid-west Greece, on the Island of Cephalonia [(38.22° N, 20.53° E), 26 January 2014 (13:55:43 UT), $M_w = 6.0$, depth = 20 km], and [(38.25° N, 20.39° E), 3 February 2014 (03:08:45 UT), $M_w = 5.9$, depth = 10 km] [10]. We shall call the specific EQs “the 2014 Cephalonia EQ1” and “the 2014 Cephalonia EQ2”, respectively.

(3) A series of EQs which took place during 2017 in the region of the eastern Aegean Sea, between the Greek Islands of Lesvos and Kos and the Turkish Asia Minor coastline as shown in Table 1 [40]. We shall refer to the particular EQs as “the 2017 eastern Aegean Sea EQs”, or more specifically as “the Lesvos 6–7 Feb. EQs”, “the Lesvos 12 Feb. EQ”, “the Lesvos 12 June EQ”, and “the Kos 20 July EQ”.

4.1.1 The 2013 Chania EQ

One of the remote stations of our MHz–kHz EME observation network is Vamos station (see the online available supplementary material) which is located in Chania prefecture, Island of Crete, close to the epicenter of the EQ of interest. The MHz EME recordings of the Vamos station from 6 October 2013 (19:26:40 UT), to 7 October 2013 (02:56:40 UT), i.e., ~ 5.5 days before the 2013 Chania EQ, were found to present critical dynamics. Specifically, the analysis of the specific MHz time series excerpt both by the MCF analysis and the NT analysis methods showed that the criticality conditions according to both methods were satisfied [28].

Moreover, by the NT method it was found that the foreshock seismicity around the area of the 2013 Chania EQ epicenter approached criticality on 5 October 2013, i.e., ~ 1.5 day before the appearance of criticality in the MHz EME and ~ 7 days before the main EQ event occurrence [28]. Note that very few foreshock seismic events had magnitude values over 2.5 within the considered time period and the considered areas, limiting thus the accuracy in determining the time of true coincidence to $\sim \pm 1$ day. The almost simultaneous appearance of critical dynamics in those two observables (MHz EME and foreshock seismicity) suggests their close relation as observable manifestations of the same complex system at critical state [28].

4.1.2 The 2014 Cephalonia EQs

Two stations of our telemetric observation network are located close to the epicenters the 2014 Cephalonia EQs: the Cephalonia station (located on the same Island where these EQs happened) and the Zakynthos station (located on the neighboring Island of Zakynthos) (see the online available supplementary material). At this point we should mention that the Cephalonia station is insensitive to EQ preparation processes happening outside of the wider area of Cephalonia Island, as well as to EQ preparation processes leading to low magnitude EQs within the area of Cephalonia Island [10].

The analysis of the MHz EME recorded at the aforementioned two stations showed that criticality was reached simultaneously for both stations' recordings a few days before the occurrence of each earthquake (~ 2 days before the occurrence of the 2014 Cephalonia EQ1 and ~ 6 days before the 2014 Cephalonia EQ2, respectively). Both MCF and NT analysis methods led to the same conclusion [10]. Moreover, the foreshock seismicity in the wider area around the Cephalonia Island was analyzed by means of the NT method, by taking also into account the seismotectonic and hazard zoning of the Ionian Islands area near Cephalonia. The NT analysis showed that not only the foreshock seismic activity also presented critical characteristics before each event (~ 4 – 7 days before the occurrence of the 2014 Cephalonia EQ1 and ~ 1 – 2 days before the occurrence of the 2014 Cephalonia EQ2), but moreover the revealed critical process was focused on the area corresponding to the west Cephalonia zone (where the main events finally happened) [10].

Importantly, on 2 February 2014 a MHz EME time series excerpt presenting tricritical characteristics was identified by the MCF analysis method in the Cephalonia station recordings [10]. It is reminded (cf. Sect. 3.1) that the detection of critical state followed by the detection of the departure from the critical state is considered a very important combination of phenomena in terms of short-term prediction. Unfortunately, during the time that the Cephalonia station recorded a tricritical MHz signal, the Zakynthos station was not in operation; actually, it was out of operation for several hours during that specific day. This signal emerged 1 day before the occurrence of the 2014 Cephalonia EQ2 and 5 days after the CWs that were identified in the MHz EME simultaneously recorded at the Cephalonia and Zakynthos stations, indicating departure from the critical state while approaching to the second main event (cf. Sect. 3.1).

4.1.3 The 2017 eastern Aegean Sea EQs

The EME related to the 2017 eastern Aegean Sea EQs were recorded by two of the stations of our telemetric observation network (see the online available supplementary material) which are located closer to the epicenters of each one of the EQs of interest. Specifically, the station located on the Island of Lesvos recorded EME related to the Lesvos 6–7 Feb. EQs, the Lesvos 12 Feb. EQ, and the Lesvos 12 June EQ, while the station located on the Island of Rhodes recorded EME related to the Kos 20 July EQ.

By using the MCF analysis method, the following results were obtained [40]:

(a) As the three Lesvos 6–7 Feb. EQs are concerned, a CW of 1 day duration was recorded 4–5 days before the occurrence of the specific EQs, indicating that a wide heterogeneous region surrounding the finally activated neighboring faults was in critical state during the simultaneous preparation process of the three EQs.

(b) 5 days prior to the Lesvos 12 Feb. EQ, a 5 h -long excerpt of the MHz EME time series recorded at the Lesvos station reached criticality (Fig. 1). Note that the specific CW was detected ~ 10 h after the third EQ of the Lesvos 6–7 Feb. EQs.

(c) In the case of the Lesvos 12 June EQ, a CW was identified in the MHz EME recordings of the Lesvos station ~ 11.5 days before the occurrence of the EQ. Importantly, a few days after the appearance of that CW, tricritical behavior was found in the kHz EME recordings of the same station (both at the 3 kHz and 10 kHz) 7–6 days before the Lesvos 12 June EQ, indicating departure from the critical state (cf. Sect. 3.1).

(d) The MHz EME recorded at the Rhodes station were found to present criticality features for a continuous period of at least one day, 1 day before the Kos 20 July EQ. A few hours later, and only ~ 3 h before the main shock, the same station recorded a 2.5 h-long tricritical MHz EME, indicating departure from critical state.

Note that NT analysis results for the MHz EME, as well as for the foreshock seismicity have not been published yet. A more complete study concerning the precursors of the aforementioned EQs is currently under preparation. Moreover, note that the detection of critical state followed by the detection of the departure from the critical state, is considered a very important combination of phenomena in terms of short-term prediction (cf. Sect. 3.1).

4.2 Results for ULF magnetic field variations

Evidence of criticality in ULF magnetic field variations, as well as departure from critical state, have recently been reported [30,31,36,46,55,56] for a number of EQs which took place in Japan and China. Specifically, we refer to the following significant EQs:

(1) An EQ which occurred on 2008 in the Sichuan province of China, [(31°01'05" N, 103°36'05" E), 12 May 2008 (06:28:01 UT), $M = 8.0$, depth = 19 km] [46]. We shall refer to the specific EQ as “the 2008 Sichuan EQ”.

(2) A mega EQ which occurred on 2011 off the Pacific coast of Tohoku, north-central Japan, followed by a huge tsunami [(38°06' N, 142°52' E), 11 March 2011 (05:46:18 UT), $M_w = 9.0$, depth ~ 20 km] [30,55]. This EQ is a very typical oceanic EQ of the plate subduction type. We shall call the specific EQ “the 2011 Tohoku EQ”.

(3) An inland, fault-type EQ which happened on 2013 on the Island of Awaji, south of Kobe, Japan, [(3425.1' N, 13449.7' E), 12 April 2013 (20:33:17 UT), $M = 6.3$, depth ~ 15 km] [56]. We shall refer to the particular EQ as “the 2013 Kobe EQ”.

(4) A series of three fault-type EQs which occurred at a very close epicentral distance, in Southwest Japan, right under the City of Kumamoto on the Island of Kyushu, [(32.788° N, 130.704° E), 14 April 2016 (12:26:41.1 UT), $M_W = 6.2$, depth ~ 9 km], [(32.697° N, 130.720° E), 14 April 2016 (15:03:50.6 UT), $M_W = 6.0$, depth ~ 8 km], and [(32.791° N, 130.754° E), 15 April 2016 (16:25:15.7 UT), $M_W = 7.0$, depth ~ 10 km] [31,36]. We shall call these EQs as a group “the 2016 Kumamoto EQs”, while we will refer to each one of them by indicating their sequence of occurrence, i.e., by calling each one them “the 2016 Kumamoto EQ1”, “the 2016 Kumamoto EQ2”, and “the 2016 Kumamoto EQ3”, respectively.

4.2.1 The 2008 Sichuan EQ

The magnetic field data recorded at the ground-based observatory of Chengdu (CDP) (see the online available supplementary material) prior to the 2008 Sichuan EQ were analyzed using the NT analysis methods and revealed interesting results [46]:

(a) Concerning the lithospheric ULF radiation, no criticality was identified for F_z while F_h showed criticality characteristics almost 1 month (25 days) before the

EQ but only for one threshold value. On the other hand $P_{z/h}$ clearly indicated that criticality conditions were met within the time period of 25–15 days before the 2008 Sichuan EQ.

(b) Concerning the depression of ULF waves (of magnetospheric origin) observed on the ground as the ionospheric signature, Dep_h indicated that criticality conditions were reached for a number of different threshold values within the time period of 23–19 days before the 2008 Sichuan EQ while δDep_h showed marginally criticality (only for one specific threshold in each case) 6 and 4 days prior to the EQ.

It is noted that the distance of CDP station from the epicenter of the EQ is ~ 80 km. Moreover for the calculation of the analyzed ULF magnetic field quantities (see Sects. 2 and 3.2.3) the nighttime interval defined by local time (LT) = 22:00–02:00 was utilized, while the chosen frequency band was 0.005–0.01 Hz (5–10 mHz). Finally, the geomagnetic activity during the period of our analysis was rather calm so that its influence can be neglected [46].

4.2.2 The 2011 Tohoku EQ

The ULF magnetic field variations recorded prior to the 2011 Tohoku EQ have been analyzed both by the NT and the MCF analysis methods and were found to reach criticality a few days to one week before the main shock [30,55].

On one hand, the NT analysis was applied only to the ULF magnetic field quantities calculated from the recordings of the Kakioka (KAK) observatory (see the online available supplementary material) and showed that [55]:

(a) Concerning the lithospheric ULF radiation, F_h fulfilled all NT analysis criticality conditions ~ 1 week (8–6 days) before the 2011 Tohoku EQ, while F_z did not exhibit any criticality condition.

(b) Concerning the depression of ULF waves (of magnetospheric origin) observed on the ground as the ionospheric signature, Dep_h indicated that criticality conditions were reached 5–4 days before the 2011 Tohoku EQ.

Note that the distance of the magnetic observatory KAK from the EQ epicenter is ~ 300 km. Moreover, for the calculation of the analyzed ULF magnetic field quantities (see Sects. 2 and 3.2.3) the nighttime interval defined by LT = 01:00–05:00 was utilized, while the chosen frequency band was 0.03–0.05 Hz (30–50 mHz). Finally, the geomagnetic activity during the time period of analysis was characterized by two relatively small ($Dst \sim -50$ nT) storms on 1 and 11 March 2011 [55].

On the other hand, the MCF analysis was applied both to the recordings (H -component, Z -component, and total intensity F) of KAK and two more ground-based magnetic observatories located at larger distances from the EQ epicenter, Memambetsu (MMB) and Kanoya (KNY) (see the online available supplementary material). Note that the distance of each magnetic observatory from the EQ epicenter is ~ 640 km for MMB, ~ 300 km for KAK, and ~ 1300 km for KNY, respectively. The MCF analysis results showed that [30]:

(a) Only the ULF data of the nearest, to the epicenter of the EQ, KAK geomagnetic observatory presented criticality.

(b) Intermittent critical behavior was identified in the ULF H -component magnetic field variations at KAK 7 days prior to the 2011 Tohoku EQ. Additionally, two more CW were identified for the KAK H -component: one 8 days, as well as one 5 days before the EQ. However, these two CWs satisfied criticality conditions for a limited range of different values of the end of laminar region φ_l , implying questionable stability of the critical behavior. Therefore, only as indications of criticality can be taken into account. Z -component magnetic field variations recorded at KAK observatory, on the other hand, yielded only one CW with a limited range of different values of

the end of laminar region φ_l 8 days before the EQ. Interestingly, it was found to overlap in time with the corresponding CW of the H -component. No indications of criticality were obtained from the MCF analysis of the ULF total, F , magnetic field variations.

4.2.3 The 2013 Kobe EQ

The ULF magnetic field variations prior to the 2013 Kobe EQ have only been analyzed using the NT analysis method [56]. The recordings of three observatories were used: Shigaraki (SGA) (located at a distance of ~ 50 km from the epicenter of the 2013 Kobe EQ), KAK, and KNY (see the online available supplementary material). For the calculation of the analyzed ULF magnetic field quantities (see Sects. 2 and 3.2.3) the nighttime interval defined by LT = 02:30–03:30 was utilized, while the chosen frequency band was 0.005–0.01 Hz (5–10 mHz). Note that, there was a moderate geomagnetic storm on 17 March with $Dst \sim -150$ nT, while a number of weaker substorms can also be identified. Nevertheless, there weren't any noticeable magnetic field disturbances observed in the vicinity of the studied earthquake while the 17 March moderate geomagnetic storm is distant enough in time so as not to influence the NT analysis results associated with the 2013 Kobe EQ [56].

The NT analysis results of the ULF magnetic field quantities calculated from the abovementioned ULF magnetic field measurements can be summarized as follows [56]:

(a) Concerning the lithospheric ULF radiation, criticality for F_h at SGA was first observed 10 days before the 2013 Kobe EQ and critical characteristics were kept up to 2 days before the main shock, while for higher thresholds criticality appears slightly earlier (~ 2 weeks before the EQ). The KNY recordings also presented critical features in terms of F_h 6 days before the EQ of interest, while the same quantity as calculated from KAK recordings reached criticality 4 days prior to the EQ, starting even 2 weeks before the EQ occurrence for some thresholds. As far as the quantity F_z is concerned it was found to satisfy criticality conditions according to the NT method from 16 up to 11 days before the EQ for SGA recordings (cf Fig. 3) between 9 and 4 days (even 2 weeks for some thresholds) before the 2013 Kobe EQ for KAK recordings while for the KNY recordings F_z was not found to reach critical state.

(b) As related to ionospheric signature, the criticality for Dep_h was reached on 9–5 days prior to the 2013 Kobe EQ at KNY, while the criticality was marginally reached 6 days before the main shock at KAK. Whereas, there was detected no criticality for Dep_h at SGA even though it is closest to the EQ epicenter probably due to the fact that the SGA station was the one carrying the higher noise contamination. Note that this is not inconsistent with the result that criticality has been revealed for F_h at the specific station [56].

4.2.4 The 2016 Kumamoto EQs

The 2016 Kumamoto EQs have been studied in terms of critical dynamics both in terms of the NT and the MCF analysis methods [31,36]. In this case the magnetic field measurements at the KNY observatory were employed on the grounds that the specific observatory is the closest located to the epicenters of the EQs of interest (at a distance of ~ 150 km). It is noted that for a month before the EQs of interest, i.e., during the period March 15 – April 15, 2016, the values of Dst index were all in the range $[-60,35]$ nT (<http://wdc.kugi.kyoto-u.ac.jp/dstdir/>), indicating a few not very strong global disturbances of the geomagnetic field, while three-hourly Kp

index reached a max value of “6-” on 07/04/2016 (<http://www.gfz-potsdam.de/en/kp-index>) [31,36].

In the case of the NT analysis, the ULF magnetic field quantities were calculated for different combinations of the time interval of the day and the narrowband band-pass filtering band because there were no recent in-situ measurements of the EM noise in the vicinity of KNY station. The main results can be summarized as follows [31]:

(a) The clearer results were obtained for the combination of the frequency band [10,20] mHz and the time interval LT = 00:00–02:00. For the specific combination, clear indications of reaching criticality within a time “window” of 1 month to 2 weeks before the Kumamoto EQs were obtained for all the analyzed ULF magnetic field characteristics.

(b) Specifically, for the lithospheric ULF radiation, F_h satisfied NT analysis critical conditions ~ 2.5 weeks before the 2016 Kumamoto EQs, while reached criticality ~ 2.5 –2 weeks before the main event.

(c) As far as the ionospheric signature of the depression of the horizontal magnetic field component is concerned, Dep_h for lower threshold values reached criticality between 29 and 26 days (~ 1 month) before the EQs of interest, while for higher thresholds criticality conditions were satisfied ~ 1 week later. Moreover, δDep_h reached criticality ~ 3 weeks before the 2016 Kumamoto EQs.

Given the NT analysis results, the unprocessed recordings of KNY station were next analyzed by means of the MCF analysis method focusing on the time period 2 weeks before the Kumamoto EQs occurrence, aiming at investigating up to which date did the critical dynamics imprints “survive” in the ULF magnetic field amplitude variations [36].

The MCF analysis revealed that the total magnetic field intensity (F) values were governed by critical dynamics a few days up to a few hours before the 2016 Kumamoto EQs [36]. Specifically, one CW was identified ~ 4 d before the 2016 Kumamoto EQ1, i.e., ~ 5 d before the 2016 Kumamoto EQ3, while one more CW was identified ~ 6 h before the 2016 Kumamoto EQ1 (and ~ 1.5 d before the 2016 Kumamoto EQ3).

Moreover, symmetry breaking appeared ~ 6.5 h after the 2016 Kumamoto EQ2 and ~ 16.5 h before the 2016 Kumamoto EQ3 (main shock), signifying the departure from critical state shortly before the occurrence of the $M_W = 7.0$ event [36]. The sequential appearance of critical dynamics followed by departure from critical state is a clear indication that the underlying system was departing the highly symmetrical state towards a low symmetry state, a state during which there is high localization of the EQ preparatory process [12,37,60]. The observed combination of phenomena can be used as a way to identify the first two strong EQs as foreshocks of an upcoming main event (cf. Sect. 3.1).

4.3 Results for VLF subionospheric propagation data

Evidence of criticality in VLF subionospheric propagation data have recently been reported [34,35] for the 2016 Kumamoto EQs (cf. Sect. 4.2) which took place in Japan. The reception of a network of 8 VLF/LF receivers spread across Japan from the JJI VLF transmitter in the southwest of the country (see the online available supplementary material), were analyzed both using the MCF [34] and the NT [35] analysis methods in order to find out any possible disturbances of the respective subionospheric propagation paths.

By analyzing the raw night-time amplitude at reception by means of the MCF method [34] it was concluded that intermittency-induced criticality was reached in the lower ionosphere from ~ 1 week to 3 days prior to the catastrophic 2016 Kumamoto

EQs. Specifically, the JJI-NSB subionospheric propagation fluctuations reached criticality on 8 days before the main event (the 2016 Kumamoto EQ3), while criticality was also identified in the JJI-IMZ and the JJI-KMK subionospheric propagation fluctuations 4 and 3 days before the main event, respectively. The obtained power-law exponent values suggest that the anti-persistency of the underlying processes was reduced while approaching the main event, as the involved processes from a wider, highly heterogeneous, preparation (activation) zone progressively presented higher focus around the fault, i.e., around an area of considerably lower heterogeneity.

On the other hand, the daily-valued VLF propagation quantities (cf. Sect. 2) calculated from the raw night-time amplitude at reception were analyzed in terms of NT [35] leading to the conclusion that lower ionosphere presented criticality possibly related to the Kumamoto EQs within the time period 10–2 days before the 2016 Kumamoto EQ3 (main event). Specifically [35]:

(a) Criticality has been revealed for all 8 stations, but for different propagation quantities (NF , DP , and TR) we have criticality for different combinations of stations and dates.

(b) The receiving stations KMK, TYH, ANA and KTU, which are all situated on the east (Pacific) coast of Japan showed either marginal or clear indications of criticality from 18 days up to 14–13 days before the main event. However, it may be possible that this behavior was related to the M5.9 EQ which happened off the Pacific Ocean coast of Japan on 01/04/2016, 02:39:08.06 UT (33.3835° N, 136.3857° E), depth = 14 km, and not to the 2016 Kumamoto EQs.

(c) After those dates, clear criticality indications were progressively appearing from 9–10 days up to 1–2 days before the 2016 Kumamoto EQs, while marginal indications of criticality were observed even on the day of the main event but only at KMK station.

(d) The clear criticality indications progressively appeared in the following order: (a) First criticality was identified in DP of the JJI-KTU path 10–8 days before the main event; (b) then, criticality appeared in the JJI-STU path (starting from 1 week before the main event in DP , and TR); (c) between 6 days and 3–2 days prior to the 2016 Kumamoto EQ3, clear criticality evidence was found in 5 propagation paths (JJI-STU, JJI-KTU, JJI-IMZ, JJI-KMK, JJI-AKT), some of them presenting critical characteristics in more than one of the analyzed quantities (TR , DP , and NF).

It is noted that the time period for which VLF subionospheric propagation anomalies were identified by the conventional nighttime fluctuation method overlaps with the criticality dates revealed by the NT analysis method, while the spatio-temporal evolution of the ionospheric perturbation associated with the Kumamoto EQs obtained by the wave-hop method matches the progressive appearance of critical dynamics in the studied receivers [35].

5 Discussion – conclusion

Based on a multidisciplinary analysis, a four-stage model of EQ dynamics by means of fracto-electromagnetic emissions (MHz–kHz EME) has recently been proposed [12]:

First stage: The initially observed MHz EM anomaly is due to the fracture of the highly heterogeneous system that surrounds the formation of strong brittle and high-strength entities (asperities) distributed along the rough surfaces of the main fault sustaining the system. The MHz EME can be described by means of a second-order phase transition in equilibrium. The appearance of the symmetry breaking phenomenon signifies the departure from critical state.

Second stage: The appearance of tri-critical behavior in the final stage of MHz EME or in the initial stage of kHz EME or in both signalizes a next distinct state of the EQ preparation process.

Third stage: The finally abruptly emerging strong sequence of kHz EM avalanches originates in the stage of stick-slip-like plastic flow namely the fracture of asperities themselves. The burst-like kHz EME does not present any footprint of a second-order transition in equilibrium.

Fourth stage: Finally the systematically observed EM silence in all frequency bands before the time of the EQ occurrence is sourced in the process of preparation of the dynamical slip which results to the fast even super-shear mode that surpasses the shear wave speed and corresponds to the observed EQ tremor.

The abovementioned model suggests four stages in the preparation of a significant EQ as observed by the sequential identification of specific dynamical and statistical properties in the fracture-induced MHz and kHz electromagnetic emissions. It has to be clarified that other EQ-related electromagnetic signals that may be generated by another physical mechanism (or combination of mechanisms) are not directly explained by the specific model. For example, as regarding the other electromagnetic signals presented in this article, namely, the possibly EQ-related ULF magnetic field anomalies and subionospheric VLF propagation anomalies, a number of different mechanisms have been suggested for their generation. Indicatively, one can refer to [17–20,33,61–63] for suggestions about the possible physical mechanisms responsible for the observed pre-EQ ULF magnetic field anomalies, as well as to [3,5,13–16,63,64] for generation mechanisms that have been suggested for the ionospheric anomalies observed prior to significant EQs.

We focus here on the first stage of the abovementioned four-stage model: The fracture-induced MHz EME are characterized by critical dynamics in analogy to a second-order phase transition in equilibrium. These EM precursors emerge during a “critical epoch” when the “short-range” correlations evolve into “long-range” ones, while an epoch of localization of the damage (departure from critical state) signalizes their cease during the second stage of the abovementioned model [12].

Importantly, it is expected that a truly preseismic MHz EM anomaly and the corresponding spatial and temporal foreshock seismic activity should constitute two sides of the same coin. Thus, the abovementioned critical features embedded in the MHz EME precursors should also be embedded in the corresponding foreshock seismic activity. As it has been shown in Section 4.1 (see also [29]), the MHz EME phenomenon behaves as a critical phenomenon while the same happens with the associated foreshock activity; the foreshock seismic activity which occurs in the region around the epicenter of the upcoming significant shock a few days up to ~one week before the main shock occurrence, and the observed MHz EME precursor which emerges during the same period, both behave as critical phenomenon. This experimental fact strongly supports the seismogenic origin of the MHz EME precursor.

The EQ preparation process has various facets which reflect to corresponding different precursors. Indifferent to the mechanisms by which they are produced, the EQ-related MHz EME, ULF magnetic field variations and subionospheric VLF propagation anomalies seem to be compatible with each other in certain aspects. The analysis of the time series of the different EM precursors presented in this review article shows that all these anomalies include the abovementioned critical features. Specifically, critical dynamics have been detected for all of them, while for some of them departure from the critical state has also been identified.

We focus on the fact that critical dynamics have been identified for all these EM phenomena a few days before the EQ occurrence (an exception is the case of ULF magnetic field variations for which criticality has been identified from a few days up to a few weeks before) while all disappear before the EQ occurrence (Fig. 5).

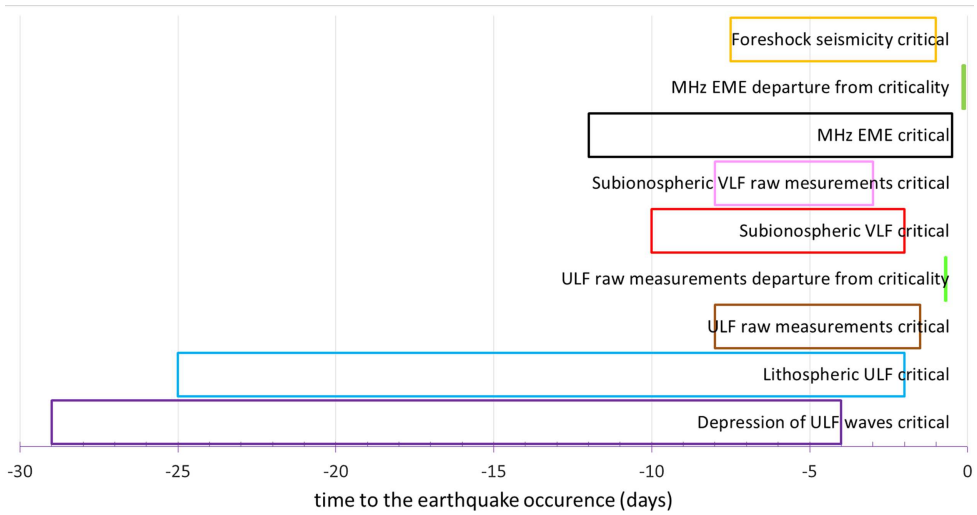


Fig. 5. Time windows prior to the EQ occurrence within which the critical dynamics features have been revealed for different EM signals as well as for foreshock seismicity based on the cases shown in Figure 4. The edges of these windows indicate the earliest and the latest time before the EQ for which the precursors of each category appear in Figure 4. (For interpretation of the references to colors, the reader is referred to the online version of this paper.)

The critical dynamics character of the aforementioned EM anomalies per se seems to provide a possible explanation for their compatibility. Importantly, the generation of all these EM precursors calls for a spatially extensive process. For example, the generation of a preseismic ionospheric anomaly requires physical and chemical transformations which occur in a spatially extended preparation (activation) zone of an impending EQ. Such a requirement is satisfied during the appearance of the “critical epoch”, i.e., the epoch during which the short-range correlations between the areas in which EQ preparation events happen have been evolved to long-range ones in an extended area; the “critical radius R ” can be estimated by the empirical relation $\log R \approx 0.5M$, where M is the EQ magnitude [65].

We emphasize that the disappearance all of the abovementioned anomalies before the EQ occurrence is also a strong compatibility indication. As it has been mentioned in Section 3.1, the appearance of symmetry breaking or tricritical dynamics following critical dynamics signatures in terms of a second order phase transition reveals the departure from the critical epoch. This can be interpreted as the transition from the phase of non-directional, almost symmetrical, distribution of events in an extensive area to a directional localized events zone. The completion of the symmetry breaking phenomenon or the tricritical dynamics signature (or the appearance of both) implies that the rupture process has already been obstructed along the backbone of strong asperities distributed across the surfaces of the main fault [12]. The strong localization of fracture process leads to the corresponding localization of the induced physical and chemical transformations which justifies the disappearance of the corresponding precursors [12].

In summary, in the frame of the revealed crucial features of critical dynamics, it could be suggested that the EM precursors considered in this article emerge during the spatially extensive phase of EQ preparation and stop when the EQ preparation becomes spatially localized around the main fault.

Publisher's Note The EPJ Publishers remain neutral with regard to jurisdictional claims in published maps and institutional affiliations.

References

1. C.H. Scholz, in *The mechanics of earthquake and faulting* (Cambridge Univ. Press, Cambridge/New York, 2002), p. 471
2. M. Hayakawa, O.A. Molchanov, *Seismo electromagnetics: lithosphere-atmosphere-ionosphere coupling* (TERRAPUB, Tokyo, 2002)
3. S. Pulinets, K. Boyarchuk, *Ionospheric precursors of earthquakes* (Springer-Verlag, Berlin/Heidelberg, 2005)
4. P.A. Varotsos, *The physics of seismic electric signals* (TERRAPUB, Tokyo, 2005)
5. O.A. Molchanov, M. Hayakawa, *Seismo electromagnetics and related phenomena: history and latest results* (TERRAPUB, Tokyo, 2008)
6. K. Hattori, in ULF geomagnetic changes associated with major earthquakes, in *Earthquake Prediction Studies; Seismo Electromagnetics* edited by M. Hayakawa (TERRAPUB, Tokyo, 2013), pp. 129–152
7. K. Eftaxias, S.M. Potirakis, *Nonlin. Processes Geophys.* **20**, 771 (2013)
8. S. Uyeda, *Proc. Jpn. Acad. Ser. B Phys. Biol. Sci.* **89**, 391 (2013)
9. M. Hayakawa, *Earthquake prediction with radio techniques* (Wiley, Singapore, 2015)
10. S.M. Potirakis, Y. Contoyiannis, N.S. Melis, J. Kopanas, G. Antonopoulos, G. Balasis, C. Kontoes, C. Nomicos, K. Eftaxias, *Nonlin. Processes Geophys.* **23**, 223 (2016)
11. S. Uyeda, T. Nagao, M. Kamogawa, *Tectonophysics* **470**, 205 (2009)
12. K. Eftaxias, S.M. Potirakis, Y. Contoyiannis, Four-Stage model of earthquake generation in terms of fracture-induced electromagnetic emissions a review, in *Complexity of Seismic Time Series: Measurement and Application*, edited by T. Chelidze, F. Vallianatos, L. Telesca (Elsevier, Oxford, UK., 2018), pp. 437–502
13. V. Korepanov, M. Hayakawa, Y. Yampolski, G. Lizunov, *Phys. Chem. Earth Parts A/B/C* **34**, 485 (2009)
14. F. Freund, *Acta Geophys.* **58**, 719 (2010)
15. S. Pulinets, D. Ouzounov, *J. Asian Earth Sci.* **41**, 371 (2011)
16. M. Hayakawa, T. Asano, A. Rozhnoi, M. Solovieva, VLF/LF sounding of ionospheric perturbations and possible association with earthquakes, in *Pre-Earthquake Processes: A Multi-Disciplinary Approach to Earthquake Prediction Studies*, edited by D. Ouzounov, S. Pulinets, K. Hattori, P. Taylor (Wiley: Indianapolis, IN, USA, 2018)
17. O.A. Molchanov, M. Hayakawa, On the generation of ULF seismogenic electromagnetic emissions, *Phys. Earth Planet. In.* **105**, 201 (1998)
18. Y. Kopytenko, V. Ismagilov, M. Hayakawa, N. Smirnova, V. Troyan, T. Peterson, *Ann. Geofisika* **44** 325 (2001)
19. K. Hattori, *Terr. Atmos. Ocean. Sci.* **15**, 329 (2004)
20. V. Surkov, M. Hayakawa, *Ultra and extremely low frequency electromagnetic fields* (Springer, Tokyo, 2014)
21. H. Kawamura, *Rev. Mod. Phys.* **84**, 839 (2012)
22. D. Sornette, *Critical Phenomena in Natural Sciences*, 2nd edn. (Springer-Verlag, Berlin/Heidelberg, 2006)
23. Y. Contoyiannis, F. Diakonos, *Phys. Lett. A* **268**, 286 (2000)
24. Y.F. Contoyiannis, F.K. Diakonos, *Phys. Rev. E* **76**, 031138 (2007)
25. Y. Contoyiannis, F. Diakonos, A. Malakis, *Phys. Rev. Lett.* **89**, 035701 (2002)
26. Y. Contoyiannis, S.M. Potirakis, K. Eftaxias, L. Contoyianni, *J. Geodynamics* **84**, 40 (2015)
27. P.A. Varotsos, N.V. Sarlis, E.S. Skordas, *Natural time analysis: the new view of time* (Springer-Verlag, Berlin/Heidelberg, 2011)
28. S.M. Potirakis, Y. Contoyiannis, K. Eftaxias, G. Koulouras, C. Nomicos, *IEEE Geosci. Rem. Sens. Lett.* **12**, 631 (2015)
29. S.M. Potirakis, A. Karadimitrakis, K. Eftaxias, *Chaos* **23**, 023117 (2013)

30. Y. Contoyiannis, S.M. Potirakis, K. Eftaxias, M. Hayakawa, A. Schekotov, *Phys. A* **452**, 19 (2016)
31. S.M. Potirakis, A. Schekotov, T. Asano, M. Hayakawa, *J. Asian Earth Sci.* **154**, 419 (2018)
32. A. Schekotov, O.A. Molchanov, K. Hattori, E. Fedorov, V.A. Gladyshev, G.G. Belyaev, V. Chebrov, V. Sinitzin, E. Gordeev, M. Hayakawa, *Phys. Chem. Earth.* **31**, 313 (2006)
33. M. Hayakawa, A. Rozhnoi, M. Solovieva, Y. Hobara, K. Ohta, A. Schekotov, E. Fedorov, *Geomatics Nat. Hazards Risk.* **4**, 275 (2013)
34. S.M. Potirakis, Y. Contoyiannis, T. Asano, M. Hayakawa, *Tectonophysics* **722**, 422 (2018)
35. S.M. Potirakis, T. Asano, M. Hayakawa, *Entropy* **20**, 199 (2018)
36. S.M. Potirakis, Y. Contoyiannis, A. Schekotov, T. Asano, M. Hayakawa, *Phys. A* **514**, 563 (2019)
37. Y. Contoyiannis, S.M. Potirakis, *J. Stat. Mech.* **2018**, 083208 (2018)
38. Y.F. Contoyiannis, F. K. Diakonou, P.G. Kapiris, A.S. Peratzakis, K.A. Eftaxias, *Phys. Chem. Earth* **29**, 397 (2004)
39. Y. Contoyiannis, S.M. Potirakis, K. Eftaxias, *Nat. Hazards Earth Syst. Sci.* **13**, 125 (2013)
40. Y. Contoyiannis, S.M. Potirakis, J. Kopanas, G. Antonopoulos, G. Koulouras, K. Eftaxias, C. Nomicos, [arXiv:1708.00320v1] (2017)
41. H.G. Schuster, *Deterministic Chaos* (VCH Publishers, Weinheim / New York, 1998)
42. F.K. Diakonou, P. Schmelcher, *Chaos* **7**, 239 (1997)
43. P. Schmelcher, F.K. Diakonou, *Int. J. Bifurcation Chaos* **7**, 2459 (1997)
44. A. Schekotov, E. Fedorov, Y. Hobara, M. Hayakawa, *J. Atmos. Electr.* **33**, 41 (2013)
45. A. Schekotov, E. Fedorov, O.A. Molchanov, and M. Hayakawa, Low frequency electromagnetic precursors as a prospect for earthquake prediction, in *Earthquake prediction studies: seismo electromagnetics*, edited by M. Hayakawa (TERRAPUB, Tokyo, 2013), pp. 81–99
46. M. Hayakawa, A. Schekotov, S.M. Potirakis, K. Eftaxias, Q. Li, T. Asano, *Open J. Earthq. Res.* **4**, 85 (2015)
47. M. Hayakawa, *Earthq. Sci.* **24**, 609 (2011)
48. P.A. Varotsos, N.V. Sarlis, E.S. Skordas, *Practica Athens Acad.* **76**, 294 (2001)
49. P.A. Varotsos, N.V. Sarlis, E.S. Skordas, *Phys. Rev. E* **66**, 011902 (2002)
50. P.A. Varotsos, N.V. Sarlis, H.K. Tanaka, E.S. Skordas, *Phys. Rev. E* **72**, 041103 (2005)
51. S. Abe, N.V. Sarlis, E.S. Skordas, H.K. Tanaka, P.A. Varotsos, *Phys. Rev. Lett.* **94**, 170601 (2005)
52. P.A. Varotsos, N.V. Sarlis, E.S. Skordas, S. Uyeda, M. Kamogawa, *Proc. Nat. Acad. Sci.* **108**, 11361 (2011)
53. P.A. Varotsos, N.V. Sarlis, E.S. Skordas, H.K. Tanaka, M.S. Lazaridou, *Phys. Rev. E* **73**, 031114 (2006)
54. N.V. Sarlis, E.S. Skordas, P.A. Varotsos, *Europhys. Lett.* **96**, 28006 (2011)
55. M. Hayakawa, A. Schekotov, S. Potirakis, K. Eftaxias, *Proc. Japan Acad. Ser. B* **91**, 25 (2015)
56. S.M. Potirakis, K. Eftaxias, A. Schekotov, H. Yamaguchi, M. Hayakawa, *Ann. Geophysics* **59**, S0317 (2016)
57. N.V. Sarlis, E.S. Skordas, M.S. Lazaridou, P.A. Varotsos, *Proc. Japan Acad. Ser. B* **84**, 331 (2008)
58. A. Rozhnoi, M. Solovieva, M. Hayakawa, VLF/LF signals method for searching of electromagnetic earthquake precursors, in *Earthquake Prediction Studies: Seismo Electromagnetics*, edited by M. Hayakawa (TERRAPUB, Tokyo, 2013), p. 31
59. A. Rozhnoi, M. Solovieva, B. Levin, M. Hayakawa, V. Fedun, *Nat. Hazards Earth Syst. Sci.* **14**, 2671 (2014)
60. Y.F. Contoyiannis, P.G. Kapiris, K.A. Eftaxias, *Phys. Rev. E* **71**, 066123 (2005)
61. K. Hattori, *Terr., Atmos. Ocean. Sci. J.* **15**, 329 (2004)

62. F. Freund, S. Pilorz, Electric Currents in the Earth Crust and the Generation of Pre-Earthquake ULF Signals in *The frontier of EQ prediction studies*, edited by M. Hayakawa, (Nihon Senmontosho Publ., Tokyo, 2012)
63. F. Freund, G. Ouillon, J. Scoville, D. Sornette, [arXiv:[1711.01780](https://arxiv.org/abs/1711.01780)] (2017)
64. A. Namgaladze, M. Karpov, M. Knyazeva, J. Atmos. Terr. Solar Phys. **171**, 83 (2018)
65. D. Bowman, G. Quillon, C. Sammis, A. Sornette, D. Sornette, J. Geophys. Res. **103**, 24359 (1998)